Numerical simulation of the magnetoresistance effect controlled by electric field in p–n junction

Pan Yang(杨盼), Wen-Jie Chen(谌文杰), Jiao Wang(王娇), Zhao-Wen Yan(闫兆文), Jian-Li Qiao(乔坚栗), Tong Xiao(肖彤), Xin Wang(王欣), Zheng-Peng Pang(庞正鹏), and Jian-Hong Yang(杨建红)†

Institute of Microelectronics, School of Physical Science and Technology, Lanzhou University, Lanzhou 730000, *China*

(Received 23 September 2015; revised manuscript received 7 December 2015; published online 25 February 2016)

The magnetoresistance effect of a p–n junction under an electric field which is introduced by the gate voltage at room temperature is investigated by simulation. As auxiliary models, the Lombardi CVT model and carrier generation-recombination model are introduced into a drift-diffusion transport model and carrier continuity equations. All the equations are discretized by the finite-difference method and the box integration method and then solved by Newton iteration. Taking advantage of those models and methods, an abrupt junction with uniform doping is studied systematically, and the magnetoresistance as a function of doping concentration, SiO_2 thickness and geometrical size is also investigated. The simulation results show that the magnetoresistance (MR) can be controlled substantially by the gate and is dependent on the polarity of the magnetic field.

Keywords: magnetoresistance, p–n junction, newton iteration

PACS: 73.43.Qt, 75.40.Mg, 02.60.Cb **DOI:** 10.1088/1674-1056/25/4/047306

1. Introduction

In view of the physical interest and potential applications, magnetoresistance (MR) effects have attracted a lot of theoretical and experimental attention. MR effects can be achieved by using non-magnetic materials such as doped silicon,[1] GaAs,[2] and magnetic materials.[3,4] However, compared with magnetic material, non-magnetic material has a large MR ratio and the resistivity increases approximately linearly with the external magnetic field, which makes the non-magnetic material more attractive to random access memory, ultrasensitive magnetic field sensors,[5] logic devices,[6,7] etc. By virtue of long spin coherence[8,9] and compatibility with the current CMOS technology, silicon is a promising material for investigating the magnetoresistance effect.

Many researches based on doped silicon have been carried out to explore the effect. Michael *et al*. have reported that the large positive magnetoresistance effect can be induced by breaking the quasi-neutrality of the space-charge effect.[10] While another mechanism was also proposed, i.e., the magnetoresistive effect can be achieved by shrinking the acceptor wave functions in the direction perpendicular to the magnetic field.[11] Meanwhile, it can also be achieved by the process of impact ionization[12] which is controlled by magnetic field.

However, a few methods are put forward to regulate MR when the magnetic field is fixed. Though varying the geometrical size[13] can achieve it, it is inconvenient for practical applications. In the present work, the magnetoresistance effect of the p–n junction induced by the space-charge effect under an electric field is studied by simulation. The results show that a wide range of magnetoresistance can be controlled, which implies that it is a more potential method to adjust magnetoresistance by using the electric field which is introduced by gate voltage.

2. Theoretical method and formulas

Classical p–n theories proposed by Shockley[14] are basic to analyse the properties of the p–n junction. This theory consists of a set of fundamental equations, which need to be modified slightly when they are used to simulate the properties of p–n under the external magnetic field and electric field.

$$\frac{\partial n}{\partial t} - \frac{1}{q}\nabla \cdot \boldsymbol{J}_{\mathrm{n}}^{*} + R = 0, \tag{1}$$

$$\frac{\partial p}{\partial t} + \frac{1}{q}\nabla \cdot \boldsymbol{J}_{\mathrm{p}}^{*} + R = 0, \tag{2}$$

$$\nabla \cdot (\varepsilon \nabla(\phi)) = q(n - p + N) - Q_{\mathrm{T}}, \tag{3}$$

$$\boldsymbol{J}_{\mathrm{n}}^{*} = \frac{1}{1 + (\mu_{\mathrm{n}}^{*} B)^2}\left[(q\mu_{\mathrm{n}} n\boldsymbol{E} + qD_{\mathrm{n}}\nabla n) + \mu_{\mathrm{n}}^{*}\boldsymbol{B} \times (q\mu_{\mathrm{n}} n\boldsymbol{E} + qD_{\mathrm{n}}\nabla n)\right], \tag{4}$$

$$\boldsymbol{J}_{\mathrm{p}}^{*} = \frac{1}{1 + (\mu_{\mathrm{p}}^{*} B)^2}\left[(q\mu_{\mathrm{n}} n\boldsymbol{E} + qD_{\mathrm{p}}\nabla p) + \mu_{\mathrm{p}}^{*}\boldsymbol{B} \times (q\mu_{\mathrm{p}} p\boldsymbol{E} + qD_{\mathrm{p}}\nabla p)\right]. \tag{5}$$

Equations (1) and (2) are the continuity equations of current for electron and hole. Here, n and p are the electron and hole density respectively, R represents the net recombination rate (including the Shockley–Read–Hall recombination rate and Auger recombination rate), and q denotes the elementary charge. Equation (3) is the electrostatic equation which is also known as the Poisson equation, whereas the permittivity, φ is the electric potential and N is the ionized net doping concentration, Q_{T} represents the charge due to traps and defects

†Corresponding author. E-mail: yangjh@lzu.edu.cn

© 2016 Chinese Physical Society and IOP Publishing Ltd

with setting Q_T to be zero). Equations (4) and (5) give the electron and the hole current density, which are modified when the magnetic field is perpendicular to the current densities,[15] here, μ_n and μ_p are the electron and hole drift mobility, μ_n^* and μ_p^* are the electron and hole Hall mobility, which are assumed to be proportional to the drift mobility[16] ($\mu_n^* = 1.2\mu_n$, and $\mu_p^* = 1.2\mu_p$), and D_n and D_p denote the electron and hole diffusion coefficient.

To obtain accurate results, the Lombardi CVT Model,[17] which contains the effect of a transverse field, doping- and temperature-dependent carrier mobility, is used. In this model, the mobility is given by three components that are composed according to the Matthiessen rule:

$$\frac{1}{\mu} = \frac{1}{\mu_{ac}} + \frac{1}{\mu_b} + \frac{1}{\mu_{sr}}. \tag{6}$$

On the right-hand side of Eq. (5), the first component μ_{ac} is the mobility limited by surface phonon scattering, and μ_b is the mobility determined by both doping concentration and temperature. The final component μ_{sr} takes into account the surface roughness scattering. More details are shown in Ref. [17].

For numerical simulation of a semiconductor device, the carrier generation-recombination is the crucial process that must be considered. In this paper, Shockley–Read–Hall recombination[18] and Auger recombination[19] within the bulk of the semiconductor are adopted.

$$R^{\mathrm{SRH}} = \frac{pn - n_i^2}{\tau_n\left[p + n_i \exp\left(\frac{E_i - E_t}{kT}\right)\right] + \tau_p\left[n + n_i \exp\left(\frac{E_t - E_i}{kT}\right)\right]}, \tag{7}$$

$$R^{\mathrm{AU}} = \left(nC_n + pC_p\right)\left(np - n_i^2\right). \tag{8}$$

Here, E_i and E_t give the intrinsic Fermi level and trap energy level respectively. For simplicity, we assume that the energy level of trap centers overlaps with the intrinsic Fermi level. τ_n and τ_p are the electron and hole lifetime, respectively. Owing to the fact that electron and hole may recombine or be generated at interfaces, τ_n and τ_p need to be modified[20] when Shockley–Read–Hall recombination is used at interfaces. Equation (8) gives the Auger recombination rate. In Eq. (8), C_n and C_p are Auger coefficients for electron and hole, n_i is the intrinsic carrier concentration given by Boltzmann statistics, n and p are the electron and hole densities, which can be given by the Boltzmann approximation.

During numerical simulation, several boundary conditions (ohmic contacts, insulated contacts, Neumann boundaries) must be considered. To implement ohmic contacts, Dirichlet boundary conditions, where surface potential, electron concentration and hole concentrations are fixed, are taken into account. In the oxide region, the zero normal current condition ($\boldsymbol{J}_n \cdot \boldsymbol{s} = \boldsymbol{J}_p \cdot \boldsymbol{s} = 0$) is imposed.[16] To ensure that the current only flows out of the p–n junction through the contact, Neumann boundaries are adopted.

To discretize those equations, the finite-difference method and the box integration method are used in order to solve them in an appropriate mesh. After discretization, the Newton iteration is used to solve the partial differential equations. The SGFramework,[21] a highly flexible partial differential equations solver, is introduced.

The structure simulated is shown in Fig. 1. Aluminum film is used to form an Ohmic contact. In order to implement a controllable electric field, SiO_2 film is formed above the p–n junction surface and then an electrode gate is formed in sequence (shown in Fig. 1). It is convenient to analyze the effect of an abrupt p–n junction with uniform doping under an electric field and magnetic field at room temperature. The simulation parameters are shown in Table 1.

Table 1. Simulation parameters.

Parameter	Value
Temperature (T)	300 K
Dielectric constant (ε_{Si})	11.8
Dielectric constant (ε_{SiO_2})	3.9
Acceptor concentration (N_A)	10^{14} cm^{-3}
Donor concentration (N_D)	10^{14} cm^{-3}
SiO_2 thickness (d)	0.1 μm

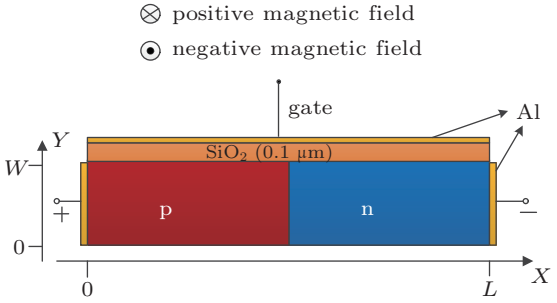


Fig. 1. (color online) Schematic diagram of the p–n junction device, where the length L is 10 μm and width W is 5 μm.

3. Numerical results and discussion

Figure 2 shows the I–V characteristics of the p–n junction at $T = 300$ K for various magnetic fields. Curent is gradually suppressed with increasing magnetic field due to the drastic change of the space-charge region. In order to describe the variation of current with applied magnetic field, here the magnetoresistance (MR) ratio is defined as $\mathrm{MR}(\%) = [R(B) - R(0)]/R(0) \times 100\%$, where $R(0)$ and $R(B)$ are the resistance (V/I) at zero and applied magnetic field. The inset

in Fig. 2 shows the MR curve at $V_{\rm bias} = 0.9$ V. It is fitted well with the parabolic relation (MR $\propto (\mu B)^2$), which is similar to the results reported in Ref. [13].

Figure 3(a) demonstrates the space-charge regions of p-type silicon and n-type silicon. Its spatial distribution of electric field is homogeneous. However, when an external magnetic field is applied, the homogeneous distribution is broken. As indicated in Fig. 3(b), when a positive magnetic field is applied, holes and electrons are attracted to the surface of the sample by the Lorenz force and accumulate. The spatial distribution and width of the space-charge region change. It is analogical to the scenario of applying a negative magnetic field.

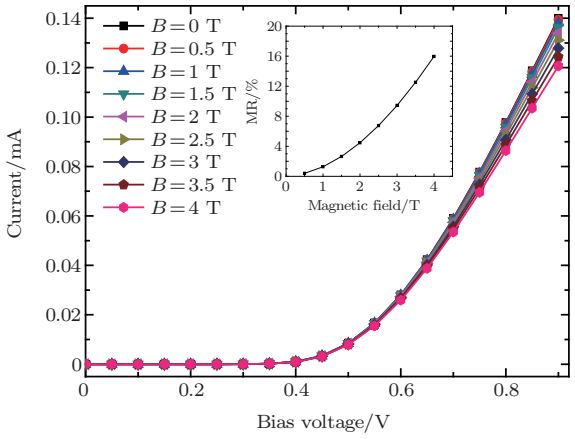


Fig. 2. (color online) I–V characteristics of the p–n junction at $T = 300$ K for various magnetic fields. The inset demonstrates MR at $V_{\rm bias} = 0.9$ V.

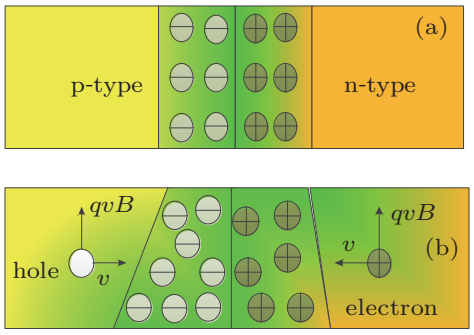


Fig. 3. (color online) Spatial distributions of space-charge region induced by the magnetic field (the colour has no special implication) for the cases (a) without magnetic field and (b) with positive magnetic field.

Figures 4(a) and 4(b) display the net charge concentrations of the space-charge region at $y = 2.5$ μm and $y = 0.3$ μm. As illustrated, there is no apparent distinction from the distribution of net charge concentration at $y = 2.5$ μm for different magnetic fields, however, a dramatic change appears at $y = 0.3$ μm (the difference between the distribution of net charge concentration at $x = 0$ μm and that at $x = 10$ μm is induced by the carriers injected). The width of the space-charge region far from the gate ($y = 0.3$ μm), compared with that under the condition without magnetic fields, increases but near the gate region decreases when we apply a positive magnetic field, the shape of the space-charge region changes from rectangular to trapezoid (Fig. 3(b)), which is well matched to the result reported by Wan *et al.*[13] Moreover, it is clearly observed that the net charge concentration changes drastically in the p-type but slightly in the n-type. It can be considered to be due to the different properties about hole and electron, which leads to various performances of magnetic field.

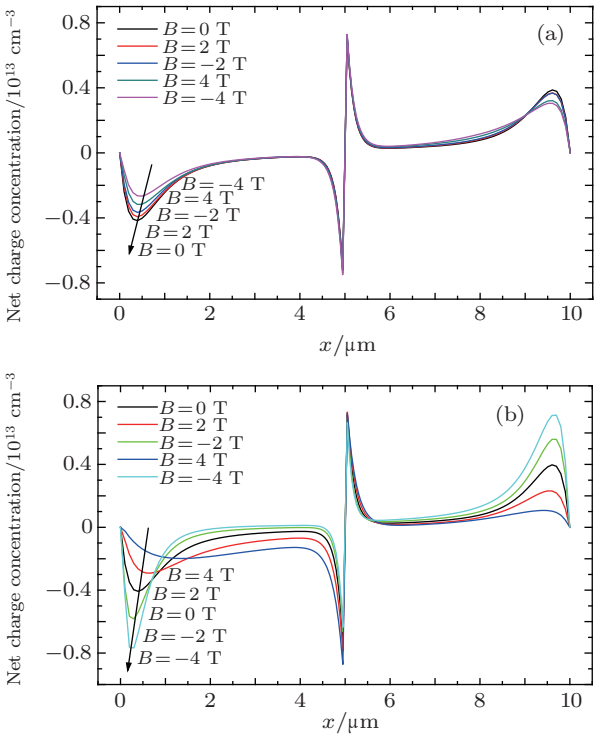


Fig. 4. (color online) Net charge concentrations for various magnetic fields at $V_{\rm bias} = 0.9$ V, $y = 2.5$ μm (a) and 0.3 μm (b).

In order to discuss the magnetoresistance effect of the p–n junction under an electric field clearly, here, the MR ratio is modified into $M_1(\%) = [R(B, V_{\rm gate}) - R(0)]/R(0) \times 100\%$, where $R(0)$ and $R(B, V_{\rm gate})$ are the resistance (V/I) at zero applied magnetic field and that at applied magnetic field B and gate voltage $V_{\rm gate}$. MR$_1$ can also be given by MR$_1$ = MR + $\Delta R_E/R_0 + f(B,E)$, where $\Delta R_E = R(B = 0\ {\rm T}, V_{\rm gate}) - R(B = 0\ {\rm T}, V_{\rm gate} = 0\ {\rm V})$ is the resistance variation ($B = 0$ T). MR and $\Delta R_E/R_0$ are the resistance variation ratios without gate voltage and without magnetic field respectively, $f(B,E)$ is an interaction term induced by the interaction between magnetic field and gate voltage.

At the zero-magnetic field, the resistance increases with an increase of negative gate voltage applied and decreases with the increase of positive gate voltage. The resistance variation ratio ($\Delta R_E/R_0$) without magnetic field is shown in Fig. 5. As indicated, $\Delta R_E/R_0$ increases and gradually tends to be saturated with negative gate voltage decreasing. When positive gate voltage is applied, $\Delta R_E/R_0$ decreases linearly with gate voltage increasing, which can be seen from the fact that the ability for $\Delta R_E/R_0$ to compensate for MR$_1$ is enhanced. The change contributes to the difference in electrical property

($\mu_n > \mu_p$) and the variation of hole and electron concentration. When positive voltage is applied to the gate, the electron concentration increases and the hole concentration decreases, resulting in the electron current increasing and the hole current decreasing. Whereas the increase of electron current dominates the decrease of hole current because of $\mu_n > \mu_p$, thus the total current increases, which indicates the decrease of resistance. It is opposite to the scenario of applying negative gate voltage.

To explore the variation of $f(B,E)$, the force analysis of hole under magnetic field and gate voltage is shown in Fig. 6. (The electron is not shown because a slight change occurs in the n-type. The colour has no special implication.) As displayed, when condition (a) (Fig. 6(a)) and condition (d) (Fig. 6(d)) are imposed on the device, the Lorentz force and electric field force =both contribute to the spatial variation of hole concentration and electric field inhomogeneity of the space-charge region in the p-type region, whereas carriers move toward the same orientation, resulting in carrier scattering aggravating, leading to $f(B,E) < 0$ (compensating for MR). However, for the conditions (b) and (c), the Lorentz force and electric field force compete with each other, the $f(B,E)$ depends on the stronger of the two forces. When electric field force qE_e dominates Lorentz force qvB, the compensating effect occurs.

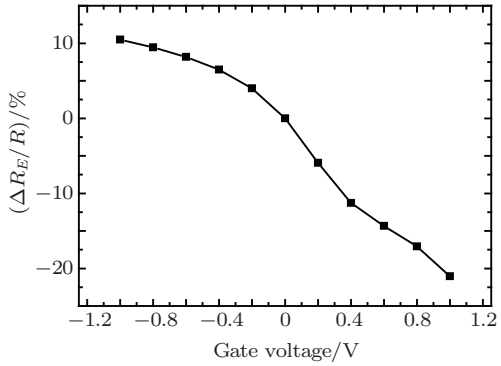


Fig. 5. Variation of resistance ratio with gate voltage at $B = 0$ T and $V_{bias} = 0.9$ V.

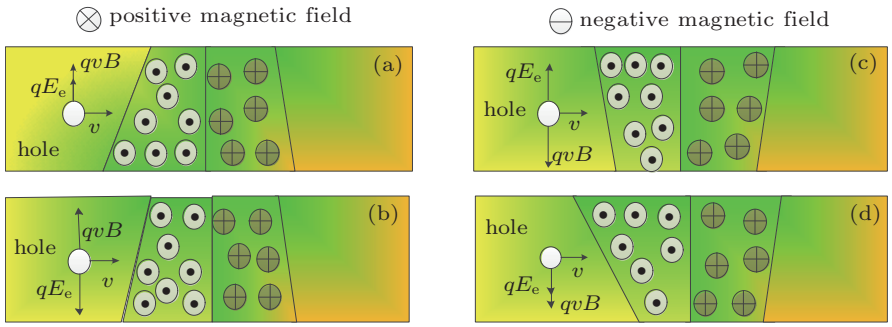


Fig. 6. (color online) The spatial distributions of space-charge region with different conditions: (a) with positive magnetic field and negative gate voltage; (b) with positive magnetic field and gate voltage; (c) with negative magnetic field and negative gate voltage; (d) with negative magnetic field and positive gate voltage. The qvB is the Lorentz force and qE_e is the electric field force.

On the basis of the above discussion, the results shown in Fig. 7 can be easily understood. As shown in Fig. 7, at a low magnetic field without gate voltage ($\Delta R_E/R_0 = f(B,E) = 0$), MR_1 shows an approximately quadratic relationship and is symmetrical about $B = 0$ T. Whereas with the absolute value of gate voltage increasing, the symmetry of MR_1 curves is gradually broken because of $f(B,E) \neq 0$. It demonstrates that MR is dependent on the polarity of magnetic field, which is different from other results.[10–13]

In addition, it can also be noted that the MR is about 0.396% with a magnetic field of 0.5 T and an applied bias voltage of 0.9 V, while an 11.107% magnetoresistance ratio is achieved with a negative gate voltage of −1 V at the same bias voltage. The MR is enlarged substantially due to the contribution of $\Delta R_E/R_0$ ($f(B,E)$ is small.) However, the distinction of the magnetoresistance curve between various negative gate voltages disappears with magnetic field increasing and gate voltage decreasing. It can be explained by the fact that the $\Delta R_E/R_0$ tends to be saturated which is shown in Fig. 5. For a positive gate voltage, the magnetoresistance ratio can reach −1.740% when 0.2 V is applied to the gate with $B = 2$ T for a bias of 0.9 V, but the magnetoresistance ratio reaches 4.477% when only magnetic field $B = 2$ T is applied. The difference is induced by the compensating of $\Delta R_E/R_0$ and $f(B,E)$ for magnetoresistance, which makes the magnetoresistance reduced. While $f(B,E)$ becomes more important with positive gate voltage increasing, which can be seen from the degree of symmetry breaking.

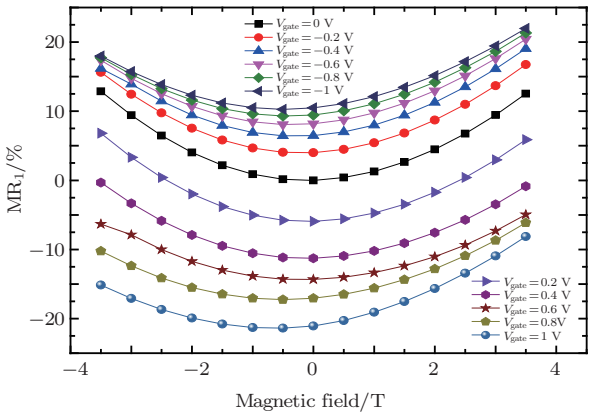


Fig. 7. (color online) Variations of MR_1 with magnetic field for various gate voltages at a bias voltage of 0.9 V.

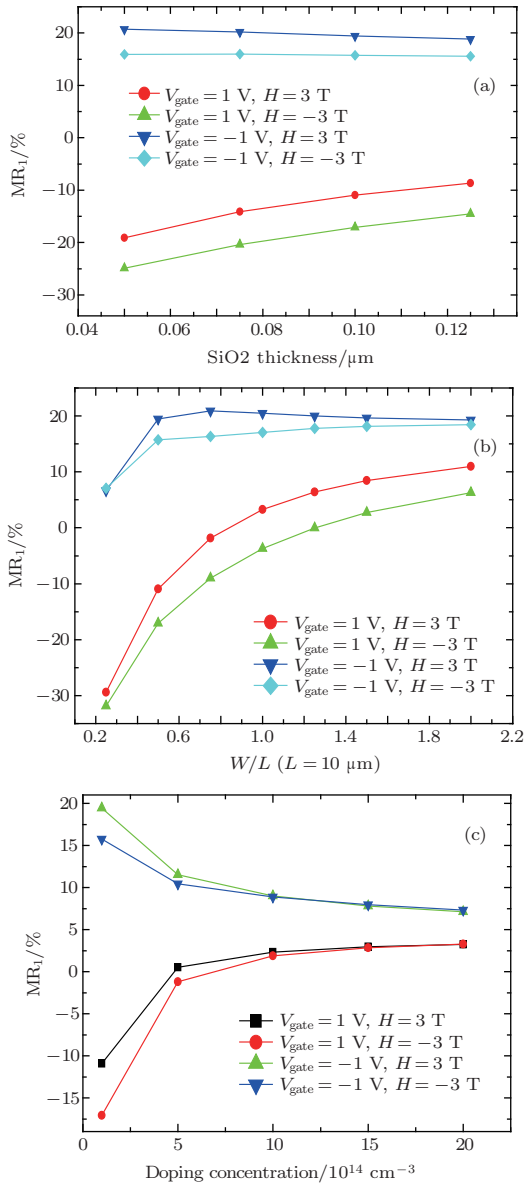


Fig. 8. (color online) Variations of MR_1 with (a) SiO_2 thickness with $W = 5$ μm, $L = 10$ μm, and $N_A = N_D = 1 \times 10^{14}$ cm^{-3}, (b) W/L with SiO_2 thickness $d = 0.1$ μm, $L = 10$ μm, and $N_A = N_D = 1 \times 10^{14}$ cm^{-3}, (c) doping concentration ($N_A = N_D$) with $W = 5$ μm, $L = 10$ μm, and $N_A = N_D = 1 \times 10^{14}$ cm^{-3}. A bias voltage of 0.9 V is applied at $T = 300$ K under conditions in panels (a), (b), and (c).

Figure 8 shows variations of magnetoresistance with SiO_2 thickness, W/L and doping concentration respectively. As indicated in Fig. 8(a), with SiO_2 thickness increasing, magnetoresistance increases linearly because of the compensation capabilities of $\Delta R_E/R_0$ reducing when positive gate voltage is applied and decreases slightly with applied negative voltage increasing due to $\Delta R_E/R_0$ reducing. On account of $f(B,E) \neq 0$, the intervals of MR_1 curves occur when different polar magnetic fields are applied at the same gate voltage. Figure 8(b) displays the variations of magnetoresistance with W/L for different values of V_{gate} and B. The magnetoresistance tends to be saturated with W/L increasing. It derives from MR tending to saturation[10] and $\Delta R_E/R_0$ gradually decreasing to zero due to the fact that the electric field diminishes with W increasing. The variations of magnetoresistance with doping concentration are shown in Fig. 8(c). There is some evidence that magnetoresistance would be saturated at high doping concentration. The carrier scattering aggravating is the significant mechanism, which makes MR and $f(B,E)$ gradually decrease to zero.

4. Conclusions

In this paper, the magnetoresistance effect of the p–n junction under an electric field at room temperature is simulated. The results indicate that it is a useful method to control magnetoresistance by gate voltage. A larger MR can be achieved by negative gate voltage, and it can also be compensated by positive gate voltage. Meanwhile, MR is dependent on the polarity of magnetic field when gate voltage is applied. Furthermore, the doping concentration, SiO_2 thickness and p–n junction size are also investigated. The results will promote the applications of silicon-based magnetoresistance devices such as a reconfigurable logic device based on magnetoresistance, access memories, and so on.

References

[1] Yang D Z, Wang F C, Ren Y, Zuo Y L, Peng Y, Zhou S M and Xue D S 2013 *Adv. Funct. Mater.* **23** 2918
[2] Sun Z G, Mizuguchi M, Manago T and Akinaga H 2004 *Appl. Phys. Lett.* **85** 5643
[3] Zhao J J, Lu Y, Haosibayar, Ru X, Yang R F, Li Q A, Sun Y and Cheng Z H 2008 *Chin. Phys. B* **17** 2717
[4] Liu W, Liu X H, Cui W B, Gong W J and Zhang Z D 2013 *Chin. Phys. B* **22** 027104
[5] Lu J D, Hou Y L, Xiong Z Z, Hou T P and Wei R 2008 *Microelectronics Journal* **39** 1576
[6] Luo Z C, Zhang X Z, Xiong C Y and Chen J J 2015 *Adv. Funct. Mater.* **25** 158
[7] Joo S, Kim T, Shin S H, Lim J Y, Hong J, Song J D, Chang J, Lee H W, Rhie K, Han S H, Shin K H and Johnson M 2013 *Nature* **494** 72
[8] Appelbaum I, Huang B Q and Monsma D J 2007 *Nature* **447** 295
[9] van't Erve O M J, Hanbicki A T, Holub M, Li C H, Affouda C and Thompson P E 2007 *Appl. Phys. Lett.* **91** 212109
[10] Michael P Delmo, Shinpei Yamamoto, Shinpei Kasai, Teruo Ono and Kensuke Kobayashi 2009 *Nature* **457** 1112
[11] Schoonus J J H M, Haazen P P J, Swagten H J M and Koopmans B 2009 *J. Phys. D: Appl. Phys.* **42** 185011
[12] Schoonus J J H M, Bloom F L, Wagemans W and Swagten H J M and Koopmans B 2008 *Phys. Rev. Lett.* **100** 127202
[13] Wan C H, Zhang X Z, Gao X L, Wang J M and Tan X Y 2011 *Nature* **477** 304
[14] Shockley W 1949 *Bell Syst. Tech. J.* **28** 435
[15] Andor L, Henry P B, Nathan A and Schmidt-Weinmar H G 1985 *IEEE Trans. Electron Dev.* **ED-32** 1224
[16] Walter Allegretto, Arokia Nathan and Henry Baltes 1991 *IEEE Trans. Comput.-aided Design* **10** 501
[17] Claudio Lombardi, Stefano Manzini, Antonio Saporito and Massimo Vanzi 1988 *IEEE Trans. Comput.-aided Design* **7** 1164
[18] Shockley W and W T 1952 *Read Phys. Rev.* **87** 835
[19] Hall R N 1952 *Phys. Rev.* **87** 387
[20] Grove A S 1967 *Physics and Technology of Semiconductor Devices* (New York: Wiley)
[21] Kramer K M and Hitchon W N 1997 *Semiconductor Devices: a Simulation Approach* (Prentice Hall PTR, 1997)